Modeling plant transpiration under limited soil water: comparison of different plant and soil hydraulic parameterizations and preliminary implications for their use in land surface models

www.reading.ac.uk/centaur

CentAUR

Central Archive at the University of Reading

Reading's research outputs online
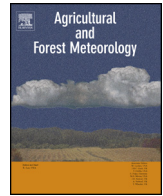
Modeling plant transpiration under limited soil water: Comparison of different plant and soil hydraulic parameterizations and preliminary implications for their use in land surface models

Anne Verhoef [a],[*], Gregorio Egea [b]

[a] Department of Geography and Environmental Science; School of Archaeology, Geography and Environmental Science, The University of Reading, Whiteknights, PO Box 227, Reading RG6 6AB, UK
[b] Area of Agroforestry Engineering, Technical School of Agricultural Engineering, University of Seville, Ctra. Utrera, km 1, 41013 Seville, Spain

ARTICLE INFO

ABSTRACT

Accurate estimates of how soil water stress affects plant transpiration are crucial for reliable land surface model (LSM) predictions. Current LSMs generally use a water stress factor, β, dependent on soil moisture content, θ, that ranges linearly between $\beta = 1$ for unstressed vegetation and $\beta = 0$ when wilting point is reached. This paper explores the feasibility of replacing the current approach with equations that use soil water potential as their independent variable, or with a set of equations that involve hydraulic and chemical signaling, thereby ensuring feedbacks between the entire soil–root–xylem–leaf system. A comparison with the original linear θ-based water stress parameterization, and with its improved curvi-linear version, was conducted. Assessment of model suitability was focused on their ability to simulate the correct (as derived from experimental data) curve shape of relative transpiration versus fraction of transpirable soil water. We used model sensitivity analyses under progressive soil drying conditions, employing two commonly used approaches to calculate water retention and hydraulic conductivity curves. Furthermore, for each of these hydraulic parameterizations we used two different parameter sets, for 3 soil texture types; a total of 12 soil hydraulic permutations. Results showed that the resulting transpiration reduction functions (TRFs) varied considerably among the models. The fact that soil hydraulic conductivity played a major role in the model that involved hydraulic and chemical signaling led to unrealistic values of β, and hence TRF, for many soil hydraulic parameter sets. However, this model is much better equipped to simulate the behavior of different plant species. Based on these findings, we only recommend implementation of this approach into LSMs if great care with choice of soil hydraulic parameters is taken.

Crown Copyright © 2014 Published by Elsevier B.V. Open access under CC BY license.

1. Introduction

Most land surface models (LSMs), i.e. those models describing the land-surface atmosphere interactions in Numerical Weather Prediction (NWP) models or Global Circulation Models (GCMs), now employ coupled net assimilation (A_n)–stomatal conductance (g_s) descriptions (Sala and Tenhunen, 1996; Arora, 2003; Calvet et al., 2004; Keenan et al., 2009; Sellers et al., 1996; Best et al., 2011; Boussetta et al., 2013; Oleson et al., 2013; Van Den Hoof et al., 2013). These models ensure the most realistic representation of plant physiological processes, which in theory should lead to more accurate predictions of (global) water and carbon cycles, under current and future climatic conditions. For example, accurate model

simulations of heat-wave related temperature anomalies over the European domain, crucially depend on accurate soil moisture predictions (e.g. Zampieri et al., 2009), which in turn rely on realistic descriptions of canopy exchange processes in LSMs, which includes plant water stress and related root water uptake.

How the current A_n–g_s models, with some of these embedded in LSMs, take account of plant water stress is described in detail in Egea et al. (2011a), for example. In almost all LSMs water stress will be determined by making use of a key soil hydraulic property: the soil water characteristic (SWC) which describes the relationship between soil matric potential, ψ_s (e.g. in MPa) and volumetric moisture content, θ (m³ m⁻³). SWCs are generally calculated using both Brooks and Corey (1964), B&C, equations as well as Van Genuchten (1980)–Mualem (1976), VGM, parameterizations; we will get back to this in Section 2.2.

In the area of soil physics and plant science, it has long been known and widely accepted that plants respond to soil matric

potential (suction) rather than to soil water content. For example, Marshall et al., 1996; (Section 14.2) discussed the closure of leaf stomata at particular leaf water potentials and the relationship between leaf and soil water potentials. Mullins (2001) led their article by stating that "in the absence of high concentrations of solutes, [soil matric potential] is the major factor that determines the availability of water to plants". The same point can be found in Gregory and Nortcliff (2013) and in many other sources.

By contrast, in a considerable number of LSMs plant water availability directly depends on θ, despite this wealth of literature; it decreases linearly when θ decreases from its value at field capacity (FC, also called critical point, generally at $\psi_s = -0.033$ MPa[1], see e.g. Veihmeyer and Hendrickson (1931), Saxton et al. (1986), Best et al. (2011), to its value at wilting point (WP, $\psi_s = -1.5$ MPa), respectively. θ_{FC} and θ_{WP} depend on soil textural composition, and on the type of hydraulic parameterization selected (B&C versus VGM) and parameter set used, as summarized in Section 2.2 and Table 2. The plant water stress factor (although plant water availability function would be a more appropriate name), generally referred to as β, is normalized by $\theta_{FC} - \theta_{WP}$, so that β becomes dimensionless and ranges between 1 (well-watered plants) and 0 (transpiration is zero, apart from cuticular transpiration):

$$
\beta \begin{cases} 1 & \theta \geq \theta_{FC} \\ \left[\dfrac{\theta - \theta_{WP}}{\theta_{FC} - \theta_{WP}} \right] & \theta_{WP} < \theta < \theta_{FC} \\ 0 & \theta \leq \theta_{WP} \end{cases} \tag{1a}
$$

Many LSMs (e.g. Best et al., 2011, for the JULES UK community model, or Boussetta et al., 2013, for the CTESSEL model) use this linear decline function for their β parameterization.

The term $(\theta - \theta_{WP})/(\theta_{FC} - \theta_{WP})$ is also known as the fraction of transpirable soil water (FTSW). In most current LSMs, this type of β factor is being used to apply water stress directly to A_n or to the parameters of the photosynthesis model (Arora, 2003; Ronda et al., 2001; Calvet et al., 2004; Krinner et al., 2005; Best et al., 2011; Boussetta et al., 2013).

Egea et al. (2011a), from hereon referred to as EVV11, introduced a more versatile β function which varies curvi-linearly (with flexibility in degree of curvature, via parameter q, see Eq. (1b)), when θ ranges between θ_{FC} and θ_{WP}:

$$
\beta \begin{cases} 1 & \theta \geq \theta_{FC} \\ \left[\dfrac{\theta - \theta_{WP}}{\theta_{FC} - \theta_{WP}} \right]^q & \theta_{WP} < \theta < \theta_{FC} \\ 0 & \theta \leq \theta_{WP} \end{cases} \tag{1b}
$$

EVV11 also introduced alternative ways to exert water stress on canopy exchange processes, i.e. not just via stomatal (multiplication of g_s by β) or biochemical pathways (by multiplying maximum carboxylation rate, V_{cmax}, and maximum photosynthetic electron transport rate, J_{max}, with β) but also through multiplication of mesophyll conductance, g_m, by β (see also Calvet, 2000) or a combination of the above.

There are some models that calculate β as a function of soil matric potential, ψ_s. One of the earliest water stress equations of this kind is the one by Feddes et al. (1978), used in the hydrological SWAP model (Van Dam et al., 2008). Focusing on LSMs (SWAP is not a LSM; it is not embedded in a NWP or GCM), Oleson et al. (2013), from here on referred to as OEA13, for the Community Land Model

Table 1
Parameter values used in model equations, and explanation of abbreviations.

Parameter	Explanation	Default value
a_1	Parameter of D02 model, see Eq. (5)	6.0
a_{ABA}	Effective ABA sequestration rate [mol H_2O m^{-2} s^{-1}]	0.0001
$b(-)$	B&C: slope of the soil water characteristic	See Table 2
D_0	Parameter of D02 model, see Eq. (5) [kPa]	1.67
K_{sat}	B&C & VGM: saturated hydraulic conductivity [m s^{-1}]	See Table 2
$l(-)$	VGM: empirical pore-connectivity parameter	See Table 2
L_{max}	Max. xylem hydraulic conductivity [mol m^{-2} s^{-1} MPa^{-1}]	0.00667
$n(-)$	VGM; measure of the pore-size distribution	See Table 2
$R_{sr,min}$	Min. soil-root hydraulic resistance [MPa mol^{-1} H_2O m^2 s]	0.1
α	VGM; inverse of the air-entry matric potential [m^{-1}]	See Table 2
γ	ABA synthesis parameter [m^3 mol^{-1} ABA]	1.48×10^{-4}
δ	Increase in stomatal sensitivity to [ABA] [MPa^{-1}]	-2.0
θ_{sat}	Soil moisture at saturation [m^3 m^{-3}]	See Table 2
θ_{FC}	Soil moisture at field capacity (-0.033 MPa) [m^3 m^{-3}]	See Table 2
θ_{WP}	Soil moisture at wilting point (-1.5 MPa) [m^3 m^{-3}]	See Table 2
λ_r	Root ABA synthesis coefficient [MPa^{-1} m^{-2} s^{-1}]	4×10^{-6}
λ_e	Leaf ABA synthesis coefficient [MPa^{-1} m^{-2} s^{-1}]	1×10^{-6}
ψ_{tL}	Threshold value of ψ_e at which L_{re} starts to decline [MPa]	-1.0
ψ_{xL}	Value of ψ_e at which L_{re} falls to zero [MPa]	-7.0^*
$\psi_{s,sat}$	B&C: soil matric potential at air entry [MPa or m]	See Table 2
$\psi_{s,max}$	Value of ψ_s at field capacity [MPa]	-0.033

Abbreviation	Explanation
ABA	Abscisic acid
B&C	Brooks and Corey (1964)
BL	Biochemical limitation
C&H	Clapp and Hornberger (1978)
CEA	Cosby et al. (1984)
CLM	Community Land Model
D02	Dewar (2002)
EVV11	Egea et al. (2011a)
FC	Field capacity
FTSW	Fraction of transpirable soil water
LSM	Land surface model
ML	Mesophyll limitation
OEA13	Oleson et al. (2013)
PFT	Plant functional type
RT	Relative transpiration
S05	Sinclair (2005)
SL	Stomatal limitation
SWC	Soil water characteristic
SVG	Schaap and Van Genuchten (2006)
TRF	Transpiration reduction function (RT versus FTSW)
VGM	Van Genuchten-Mualem hydraulic parameterization
WEA	Wösten et al. (1999)
WP	Wilting point

[*] D02 used -3 MPa.

(CLM), define a plant wilting factor, equivalent to β in Eqs. (1a) and (1b), by:

$$
\beta = 0 \leq \frac{\psi_{s,c} - \psi_s}{\psi_{s,c} - \psi_{s,o}} \leq 1 \tag{2}
$$

where $\psi_{s,c}$ is the soil water potential at which stomata close and $\psi_{s,o}$ is the soil water potential when the stomata are fully open. In Eq. (2) the independent variable is ψ_s, not θ. Furthermore, whereas in Eqs. (1a) and (1b) parameters θ_{FC} and θ_{WP} are dependent on soil texture, $\psi_{s,o}$ and $\psi_{s,c}$ are dependent on plant functional type (PFT).

---

[1] Note that 10 kPa is another widely used value to denote FC (see, e.g. Verhoef and Egea, 2013).

Values for $\psi_{s,o}$ range from −0.35 to −0.83 MPa[2]; for $\psi_{s,c}$ Oleson et al. (2013) quote values ranging between −2.24 and −4.28 MPa. These $\psi_{s,o}$ and $\psi_{s,c}$ values are based on White et al. (2000) who collated a table of predawn leaf water potential, ψ_{lpd}, at initial and final reduction to stomatal conductance. Given no transpiration during the night, ψ_{lpd} is usually approximately equal to ψ_s (Kozlowski et al., 1991). Thus, ψ_{lpd} was used as a surrogate measure for ψ_s.

In CLM, soil water stress influences g_s directly by multiplication of the minimum conductance, g_0, by β and also indirectly through A_n. The latter effect is achieved by multiplying V_{cmax} and dark respiration by β.

Both methods described above simply make use of the SWC and empirical soil texture- or PFT-related parameters. A more sophisticated approach, where stomatal response to soil water deficit involves combined plant/soil hydraulic (not just via SWC, but also through the soil hydraulic conductivity, K, which affects the flow of water from soil to roots) and chemical signaling through abscisic acid (ABA), would potentially be much better equipped for explaining contrasting plant behavior (e.g. isohydric versus anisohydric behavior, of the diurnal minimum foliage water potential, $\psi_{f,min}$) and soil hydraulic effects. It would therefore ensure more realistic interactions and feedbacks between soil, vegetation and atmosphere in LSMs. For isohydric behavior the predicted $\psi_{f,min}$ changes little with the soil water reserve or the soil-to-plant hydraulic conductivity, whereas for anisohydric behavior the interaction between hydraulic and chemical signals is absent leading to a marked decrease in $\psi_{f,min}$ in droughted plants, as observed in sunflower and other species (Tardieu et al., 1996; Tardieu and Simonneau, 1998).

In this context, Dewar (2002; from hereon referred to as D02), following Tardieu and Davies (1993) and related papers (see D02), used an alternative water stress function:

$$\beta = \exp\left\{ -[ABA]\,\gamma\exp(\delta\psi_e) \right\} \qquad (3)$$

where [ABA] is abscisic acid concentration (mol m^{-3}), γ an ABA synthesis parameter (m^3 mol^{-1} ABA), δ is the increase in stomatal sensitivity to [ABA], in MPa^{-1}, and ψ_e the water potential of the bulk leaf epidermis (MPa), with $\delta < 0$ denoting isohydric behavior and $\delta = 0$ representative of anisohydric behavior.

Eqs. (1)–(3) represent a range of water stress functions, with various degrees of complexity and parameter requirement. The ultimate test of the suitability of the various β factors is evaluation of their ability to predict reduction in transpiration as a result of plant water stress. Factor β will determine the ratio of transpiration, E, between water stressed plants ($\beta < 1$; $E < E_{max}$, with E_{max} the maximum transpiration for the atmospheric conditions under consideration) and well-watered plants ($\beta = 1$; $E = E_{max}$): the relative transpiration, RT, which is often plotted as a function of FTSW (see e.g. Sinclair, 2005, from here on referred to as S05). Others refer to RT as a function of (normalized) soil moisture content, as the transpiration reduction function, TRF (Metselaar and De Jong Van Lier, 2007; Durigon et al., 2012; De Jong van Lier et al., 2013); we have adopted this term throughout the paper. The TRF represents three phases: the constant-rate phase, the falling-rate phase, and a relatively short transition phase in between (see Metselaar and De Jong Van Lier, 2007).

In Fig. 1 we have collated experimental evidence of the shape of the RT versus FTSW relationship (TRF) as affected by plant species, species genotypes and soil texture; these data were obtained from the literature and serve as an illustration of the range of TRFs curves present in nature. We use the general shape of these curves (in
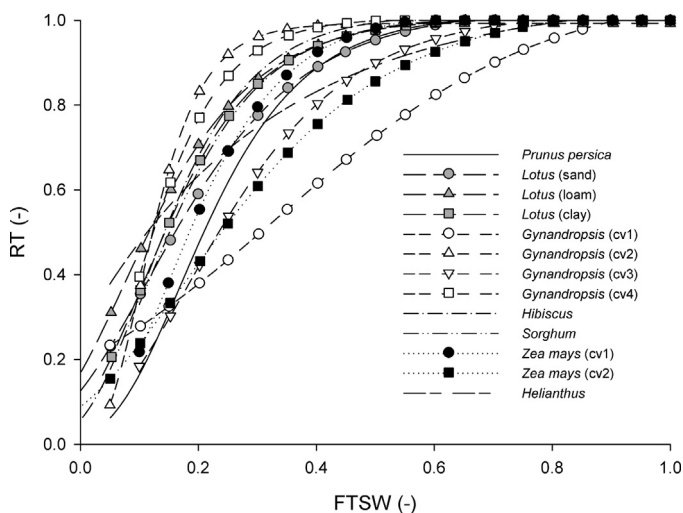

Fig. 1. Relative transpiration (RT) as a function of fraction of transpirable soil water (FTSW), determined experimentally for a number of species, cultivars and soil textures. The data are found in Gardner and Ehlig (1963) for birdsfoot (Lotus corniculatus L., cv. Tennuifolius; isohydric C₃ species, grown on 3 different soil types), Do Paço et al. (2013) for peach (Prunus persica L., cv. Silver King; isohydric C₃ species), Sinclair et al. (2005) for hibiscus (Hibiscus sp.; isohydric C₃ species), Gholipoor et al. (2012, 2013) for sorghum (Sorghum bicolor L., cv. BTX378; isohydric C₄ species) and maize (Zea mays L.; isohydric C₄ species, 2 cultivars), Masinde et al. (2005) for spiderplant (Gynandropsis gynandra L.; isohydric C₄ species, 4 cultivars) and Diaz-Espejo et al. (2005) for sunflower (Helianthus annuus L. cv. Teddybear; anisohydric C₃ species).

particular the Prunus persica (peach) curve, for reasons explained in Section 2.3) to test the ability of the models, and to guide our parameter choices. Except for Helianthus annuus (sunflower), all experiments were conducted in controlled glasshouse conditions with potted plants. In these experiments, transpiration was determined gravimetrically by weighing the plant pots on a daily basis (at the same time for well-watered and droughted species) for the duration of the soil drying cycle. FTSW was estimated as the difference between daily weight and final weight, divided by the total transpirable water (i.e. the difference between initial and final weights). The initial weight was recorded once plants were over-irrigated and let to drain overnight. The final weight was recorded when RT had decreased to less than 0.1. In the case of sunflower plants (outdoor experiment), transpiration was determined by mini-lysimetry (Diaz-Espejo et al., 2005) and FTSW was calculated from measured θ, with θ_{FC} and θ_{WP} calculated from the SWC obtained for the sandy loam soil (Fernandez-Galvez et al., 2007). The TRF for peach trees was derived by the authors from a published RT versus predawn leaf water potential (deemed a surrogate of ψ_s) relationship (Do Paço et al., 2013). The experiment was conducted on a commercial peach orchard grown under Mediterranean climatic conditions and sandy soil. FTSW was calculated from the ψ_s values by using the B&C soil parameterization (see Eqs. (16) and (17), and Table 2). The TRFs for Lotus corniculatus (birdsfoot) plants were also calculated from RT versus ψ_s relationships following the procedure described for peach trees.

Most curves in Fig. 1 display a similar shape, where plants experience no or little reduction in water availability until FTSW equals approximately 0.4, below which a steep decline in RT takes place. This agrees with numerous reports indicating that transpiration remains unchanged until a fraction of the available water is lost, after which transpiration is depleted until available soil water is exhausted (e.g. Sadras and Milroy, 1996).

Exceptions are Gynandropsis cv1 (a more or less linear decline in RT between FTSW = 1 and FTSW = 0) and Helianthus which has a much more gradual decrease in RT at lower values of FTSW (anisohydric behaviour). With regards to the effect of soil texture,

---

[2] Note that we have used a value of specific weight of water of 10,000 N m^{-3} to transfer from the units of mm, used for $\psi_{s,o}$ and $\psi_{s,c}$ in CLM, to MPa.

only Lotus data are available. These data show that the differences between TRFs are relatively small among sand, loam and clay, but that the Lotus plants on sand experienced a drop in RT at higher values of FTSW. This observation that differences between soil types are small corresponds with a modeling study, presented by S05, of RT versus FTSW curves for different soil textures, using the B&C type of SWC to derive FTSW and hydraulic conductivity (with parameters taken from Clapp and Hornberger (1978) from here on referred to as C&H).

S05 (see also Metselaar and Sinclair, 2007) calculated relative transpiration, $RT = E/E_{max}$ using (note that here we show a slightly adapted equation because we use different units for E_{max} and K_s):

$$RT = \frac{(\psi_s - \psi_e)}{[((V_w \alpha_g E_{max})/(d_{ex} K_s(\theta))) - \psi_e]} \qquad (4a)$$

with E_{max} (mol m^{-2} s^{-1}) the transpiration of well-watered plants under the same environmental conditions as those for the droughted plants, V_w the partial molar volume of water (0.000018 m^3 mol^{-1} H$_2$O), α_g a variable for geometry of soil water extraction around roots (m^2), d_{ex} the depth of soil water extraction (m) and $K(\theta)$ the soil hydraulic conductivity as a function of soil moisture content (in this case expressed as MPa^{-1} s^{-1} m^2). The results of his (S05) analysis showed that RT was essentially independent of root length density, maximum transpiration rate, and soil depth. Also, large decreases in K_s as the soil dries had only modest influences on RT.

S05 therefore simplified Eq. (4a) to:

$$RT = 1 - \frac{\psi_s}{\psi_e} \qquad (4b)$$

which, despite its simplicity, gives virtually the same values as Eq. (4a) (we confirmed this).

If we assume that $\beta \sim RT$ (if leaf temperature of the water-stressed and well-watered plants were the same then $\beta = g_s/g_{s,max} = E/E_{max}$), Eq. (4b) can be regarded as an alternative β parameterization.

De Jong van Lier et al., 2013 derived a detailed mathematical model of plant and soil hydraulics (via explicit calculation of system potentials, resistances and water flows and allowing for the effect of root geometry, but no consideration of leaf gas exchange) to derive RT. Tests showed that their prediction of RT was similar to the values calculated with the Feddes TRF; hence we have not considered their model here as simpler models are preferred for incorporation into LSMs.

This paper describes a comparison, via sensitivity analyses, of different approaches, i.e. Eqs. (1)–(4), used to represent water stress in A_n–g_s models, in order to test their suitability for incorporation into LSMs. Their appropriateness will be largely assessed from their ability to predict correct shapes of TRFs, for a range of soil textures. It will be assessed how much soil texture, by controlling soil hydraulic properties, will affect the shape of the RT curves for the different β-configurations. In this context, the effect of using different soil hydraulic parameterizations (B&C versus VGM) and different standard hydraulic parameter sets that are available in the literature will also be studied.

With this paper, using data available in the literature combined with model equations, we aim to (i) address the question whether or not plants do indeed respond more directly to matric potential rather than soil water content and (ii) whether introducing a more plant hydraulic modelling approach will capture this behaviour more accurately. A logical follow-up question is whether or not using water-stress functions based on soil matric potential, ideally combined with a plant hydraulic parameterization, rather than with soil water content as their independent variable, will improve the representation of these processes in LSMs. With the findings presented in this paper we can make an informed guess

at the implications of using these different model approaches for LSM predictions, as detailed in the Conclusions. However, via a comprehensive land surface modeling study that is currently in progress we will be able to address these implications in much more detail; these data will be presented in a follow-up paper currently in preparation.

2. Theory

2.1. Soil–plant water transport

We selected the semi-empirical A_n–g_s model as presented in Dewar (2002; D02) and Egea et al. (2011a; EVV11). Dewar introduced a guard cell model, which led to the replacement of C_s by C_i as the key CO$_2$ concentration variable (term $A_n/(C_s - \Gamma)$ was replaced by $(A_n + R_d)/C_i$):

$$g_s = g_0 + \frac{a_1(A_n + R_d)}{C_i(1 + (D_s/D_0))}\beta \qquad (5)$$

Here g_s is the stomatal conductance, g_0 the cuticular conductance (mol m^{-2} s^{-1}), A_n the leaf net CO$_2$ assimilation (mol m^{-2} s^{-1}), R_d the dark respiration rate (mol m^{-2} s^{-1}), C_i the substomatal or internal CO$_2$ concentration (μmol mol^{-1}), and D_s (kPa) the vapour pressure deficit at the leaf surface. C_i can be derived from C_c (CO$_2$ concentration at the sites of carboxylation in the chloroplasts) by using $C_i = C_c + (A_n/g_m)$, where g_m is the mesophyll conductance to CO$_2$ diffusion (i.e. from stomatal cavities to carboxylation sites).

The biochemical model for C$_3$ photosynthesis proposed by Farquhar et al. (1980) was used whereby A_n is limited by the slowest of two processes: (1) Rubisco-limited carboxylation, with maximum carboxylation rate, V_{cmax}, as key parameter; (2) light-limited carboxylation, with maximum photosynthetic electron transport rate, J_{max}, as key parameter.

D02 lists a value of 6 (based on Leuning, 1995) for parameter a_1, which, like parameter D_0 discussed below, is related to his stomatal mechanics model. EVV11 use $a_1 = 1/(1 - f_0)$, where f_0 is an empirical parameter of the stomatal conductance submodel. With a typical value of $f_0 = 0.8$ (Jacobs, 1994), we get $a_1 = 5$, which is close to Dewar's value. We have used $a_1 = 6$ in the model runs, see Table 1. D02 uses a value of $D_0 = 1.67$ kPa. Note that in the EVV11 model the variable D_* is used, which is defined as: $D_* = D_{max}/(a_1 - 1)$, with D_{max} the value of D_s when the stomata are completely closed. Jacobs (1994) uses $D_{max} = 45$ g kg^{-1} ($\sim$7.25 kPa) a typical value for agricultural crops and deciduous forest. With $a_1 = 6$ and a value of 7.3 kPa for D_{max}, we find $D_* = 1.45$ which is very similar to the value for D_0 used by Dewar (2002): 1.67 kPa. For internal model consistency we used D02's value (see Table 1).

In Eq. (5), β (–) is a water stress factor ranging between 0 and 1, for which we can use Eqs. (1)–(4). Applying water stress here is equivalent to EVV11's stomatal limitation (SL) approach. Alternatively, EVV11 accounted for the effect of water stress on the coupled A_n–g_s model by applying β to the biochemical parameters V_{cmax} and J_{max} of the photosynthesis model (BL: biochemical limitation). Finally, EVV11 also allowed for multiplication of potential or maximum (unstressed) mesophyll conductance, $g_{m,0}$, by β: mesophyll limitation (ML). They also considered a number of combinations of limitation types, and various strengths of dependencies, as denoted by parameter q in Eq. (1b). For D02 and S05 we considered water stress limitation via SL only and a combination of SL and BL for OEA13.

In β-D02 Eq. (3), the concentration of ABA [mol m^{-3}] is calculated with:

$$[ABA] = \frac{-\lambda_r \psi_r - \lambda_e \psi_e}{V_w(J_w + a)} \qquad (6)$$

Table 2
B&C and VGM type hydraulic parameters, and θ_{FC} and θ_{WP} calculated from Eqs. (16) and (19) (with ψ_s set to hydraulic head equivalents (m) of −0.033 and −1.5 MPa, respectively), for three soil textural types. Four different parameter sets were selected from the literature.

Soil texture	b (−)	θ_{sat} (m³ m⁻³)	$\psi_{s,sat}$ (m)	K_{sat} (m s⁻¹)	θ_{FC} (m³ m⁻³)	θ_{WP} (m³ m⁻³)
C&H: Clapp and Hornberger (1978)						
Sand	4.05	0.395	0.121	1.76×10^{-4}	0.175	0.068
Loam	5.39	0.451	0.478	6.95×10^{-6}	0.315	0.155
Clay	11.40	0.482	0.405	1.03×10^{-6}	0.401	0.287
CEA: Cosby et al. (1984)						
Sand	2.79	0.339	0.069	4.66×10^{-5}	0.085	0.022
Loam	5.25	0.439	0.354	3.38×10^{-6}	0.287	0.139
Clay	11.55	0.468	0.468	9.73×10^{-7}	0.395	0.283

Soil texture	θ_{sat} (m³ m⁻³)	θ_r (m³ m⁻³)	α (m⁻¹)	n (−)	l (−)	K_{sat} (m s⁻¹)	θ_{FC} (m³ m⁻³)	θ_{WP} (m³ m⁻³)
SVG: Schaap and Van Genuchten (2006)								
Sand	0.396	0.052	2.63	2.23	−1.28	2.26×10^{-6}	0.076	0.052
Loam	0.512	0.056	4.07	1.19	−6.97	3.04×10^{-6}	0.332	0.191
Clay	0.512	0.098	1.78	1.30	−5.96	2.11×10^{-7}	0.336	0.175
WEA: Wösten et al. (1999)								
Sand*	0.403	0.025	3.83	1.38	1.25	6.94×10^{-6}	0.169	0.059
Loam*	0.439	0.010	3.14	1.18	−2.34	1.40×10^{-6}	0.289	0.151
Clay*	0.614	0.010	2.65	1.10	2.50	1.74×10^{-6}	0.489	0.335

* Soil textural types based on coarse, medium and very fine in Table 4 of Wösten et al. (1999).

with λ_r and λ_e the root and leaf ABA synthesis coefficients (MPa⁻¹ m⁻² s⁻¹), respectively, ψ_r the root water potential (see Eq. (13)), J_w the soil to leaf water flux (mol m⁻² s⁻¹) and a_{ABA} the effective ABA sequestration rate [mol H₂O m⁻² s⁻¹].

J_w is described by

$$J_w = \frac{\psi_s - \psi_e}{(R_{sr} + R_{re})} \tag{7}$$

with R_{sr} and R_{re} the soil-to-root and root-to-leaf epidermis hydraulic resistances, respectively (MPa mol⁻¹ H₂O m² s). R_{re} is defined by $R_{re} = 1/L_{re}$, with L_{re} the xylem hydraulic conductivity (mol H₂O m⁻² s⁻¹ MPa⁻¹):

$$L_{re} \begin{cases} L_{max} & \psi_e > \psi_{tL} \\ L_{max} \left(\psi_e - \psi_{xL} \right) / \left(\psi_{tL} - \psi_{xL} \right) & \psi_{xL} < \psi_e < \psi_{tL} \\ 0 & \psi_e < \psi_{xL} \end{cases} \tag{8}$$

where L_{max} is the maximum of L_{re}, ψ_{tL} the threshold potential at which L_{re} starts to decline (MPa) and ψ_{xL} is the value of ψ_e at which L_{re} falls to zero (MPa).

D02 derived soil-to-root hydraulic resistance, R_{sr} (MPa mol⁻¹ m² s) from theory presented by Thornley and Johnson (1990) which led to:

$$R_{sr} = R_{sr,min} \left(\frac{\psi_s}{\psi_{s,sat}} \right)^{2+\frac{3}{b}} \tag{9}$$

with $R_{sr,min}$ the minimum soil-hydraulic resistance (MPa mol⁻¹ H₂O m² s), and $\psi_{s,sat}$ and b parameters of the B&C equation to describe the SWC (See Section 2.2). Combining Eqs. (16) and (18) (the hydraulic conductivity equation) shows that R_{sr} is equivalent to $R_{sr,min}(K_{sat}/K(\theta))$. This means that the ratio of saturated over soil moisture dependent hydraulic conductivity can be replaced by one calculated from a different parameterization, e.g. that based on VGM (see Eqs. (19) and (20)).

An alternative description for soil-to-root hydraulic resistance is given by Tardieu et al. (1992) and Tardieu and Davies (1993), here multiplied by V_w to match the units used in Eq. (9):

$$R_{sr} = V_w \frac{1}{4\pi K(\theta) L_a} \ln \left(\frac{d^2}{r^2} \right) \tag{10}$$

where $K(\theta)$ is the hydraulic conductivity as a function of soil moisture content (MPa⁻¹ s⁻¹ m²), see Eqs. (18) and (20), L_a the root length per unit area (m⁻¹), d the average half-distance among the closest roots (m), and r is the mean root diameter (m). Parameter d has been calculated with:

$$d = 0.5 r_r \sqrt{d_{soil} \pi \frac{\rho_r}{m_r}} \tag{11}$$

and L_a from:

$$L_a = \frac{m_r}{r_r^2 \pi \rho_r} \tag{12}$$

with d_{soil} the rooting depth (m), ρ_r the dry-matter density in fresh roots (kg m⁻³), r_r the mean radius of fine or active roots (mm) and m_r the mass of roots per ground area (kg m⁻²). Eqs. (11) and (12), and selected parameter values, are based on recommendations by Vince Gutschick (see http://gcconsortium.com/academic_page/index.html); for his $d_{soil} = 0.4$ m, $\rho_r = 250$ kg m⁻³, $r_r = 0.8$ mm and $m_r = 0.15$ kg m⁻², we find $L_a = 299$ m m⁻². The advantage of Eq. (10) is that it explicitly accounts for root-specific information (L_a, d and r) and it also allows for incorporation of the effects of root clumping (Tardieu et al., 1992), although this has not been studied here.

Root water potential, ψ_r, is given by:

$$\psi_r = \psi_s - R_{sr} J_w \tag{13}$$

The expression for the leaf transpiration rate is

$$E = 1.6 g_s D_s \tag{14a}$$

which will be used for the EVV11/S05/OEA13 configurations.

For the RT calculations involving β-D02 we consider the balance between the rates of xylem transport, J_w, and leaf transpiration, E, i.e. $J_w = E$:

$$\frac{\psi_s - \psi_e}{(R_{sr} + R_{re})} = 1.6 g_s D_s \tag{14b}$$

The final equation required is the CO₂ supply function

$$A_n = g_s(C_s - C_i) \tag{15}$$

2.2. Soil hydraulic parameterizations

The water retention and hydraulic conductivity curves are described by either the B&C or VGM equations. Most LSMs these days offer the option of using either or both of these parameterizations, hence this is why they were selected. Note that B&C did not set residual moisture content (see below) to zero in the water retention curve, whereas C&H did; most models using this type of functional description do so as well, so in reality we have a mixture of B&C and C&H approach (See also Marthews et al., 2014).

The B&C equation for calculation of ψ_s is given by:

$$\psi_s = \psi_{s,sat}(S_e)^{-b} \tag{16}$$

where $\psi_{s,sat}$ is the matric potential at saturation (m) and parameter b (−) denotes the slope of the SWC.

S_e is the effective saturation given by

$$S_e = \frac{\theta - \theta_r}{\theta_{sat} - \theta_r} \tag{17}$$

where θ_{sat} is the saturated soil moisture content ($m^3\,m^{-3}$) and θ_r the residual moisture content ($m^3\,m^{-3}$).

Hydraulic conductivity is calculated from

$$K(\theta) = K_{sat}S_e^{2b+3} \tag{18}$$

with K_{sat} the saturated hydraulic conductivity ($m\,s^{-1}$).

The Van Genuchten (1980) equation for the water retention curve is given by

$$\psi_s = \frac{\left(S_e^{-1/m} - 1\right)^{1/n}}{\alpha} \tag{19}$$

Parameter α (>0, in m^{-1}) is related to the inverse of the air-entry matric potential, i.e. $\psi_{s,sat}$ in Eq. (16); n (>1) is a measure of the pore-size distribution (van Genuchten, 1980); and $m = 1 - 1/n$.

The pore-size distribution model of Mualem (1976) is used for the hydraulic conductivity:

$$K(\Theta) = K_{sat}S_e^l \left[1 - \left(1 - S_e^{1/m}\right)^m\right]^2 \tag{20}$$

where K_{sat} is the hydraulic conductivity at air entry potential ($m\,s^{-1}$), and l (−) is an empirical pore-connectivity parameter.

Values for the parameters used in Eqs. (16)–(20) for four hydraulic parameter sets are presented in Table 2 and will be used in the sensitivity analysis described below. Note that we converted ψ_s from m to MPa throughout Eqs. (2), (4), (7), (9), (13), and (14b), and K to units of $MPa^{-1}\,s^{-1}\,m^2$ in Eqs. (4a) and (10). The reason for showing units of m and s in Eqs. (16)–(20) and Table 2 is related to the fact that these are SI units and more easily to interpret than in particular $MPa^{-1}\,s^{-1}\,m^2$.

2.3. Model configurations and sensitivity analyses

The resulting values of RT for the EVV11, OEA13, D02 and S05 β-parameterizations were compared under conditions of decreasing soil matric potential, i.e. a dry-down from field capacity at −0.033 MPa to beyond wilting point (−2 MPa). Parameters in the photosynthesis model were typical of almond trees (Prunus amygdalus, see EVV11 and Egea et al., 2011b), i.e. an isohydric species. Egea and colleagues have extensively measured canopy exchange in Mediterranean almond groves and hence we have reliable plant physiological parameter values available for the A_n–g_s model we employ. Unfortunately, TRF curves are not available for these almond experiments because whole-tree transpiration was not measured under severe soil water deficit. However, for the agronomic studies presented in Fig. 1 no physiological parameters were available, hence we used the

Prunus persica (Peach) TRF as verification material for the almond. We deem this appropriate because within the genus Prunus, almond is classified with the peach in the subgenus Amygdalus, and also in light of the fact that this is mainly a theoretical paper.

Driving variables varied diurnally (representing a typical clear summers's day for a Mediterranean almond orchard; the same diurnal evolution was used for each value of ψ_s, but note that model outputs between 7 a.m. and 7 p.m. only were used to calculate daily RT values, to avoid conditions of very low radiation). Air temperature varied between 17.9 and 33.6 °C, Photosynthetically Active Radiation between 202 and 2049 $\mu mol\,m^{-2}\,s^{-1}$, and relative humidity between 29% and 60%. Atmospheric CO_2 concentration was kept constant at 400 $\mu mol\,mol^{-1}$, from which C_s was derived with a wind-speed dependent leaf boundary layer resistance equation, and windspeed at 5 $m\,s^{-1}$. Surface temperature, required in the A_n model and to calculate D_s, for example, was calculated using a simple leaf surface energy balance approach.

Sensitivity analyses for *plant parameters* were only applicable to D02. ABA synthesis was considered to occur either in leaves only ($\lambda_r = 0$), roots only ($\lambda_e = 0$) or in both. Furthermore, in Eq. (3) δ was set to range from −2 to −0.5 MPa, as almond concerns an isohydric vegetation type (although $\delta = 0$, valid for anisohydric species, was shown for comparison).

Finally, a range of sensitivity analyses were performed in relation to *soil parameterization* (B&C versus VGM), and *soil parameter set* (B&C: C&H and CEA; VGM: WEA and SVG).

3. Results and discussion

3.1. Modelled TRFs; sensitivity to plant parameters

Fig. 2 shows the transpiration reduction functions (TRFs) derived from the equations presented in Sections 2.1 and 2.2, using four different β parameterizations. The set of equations comprising of Eqs. (5), (14a) or (14b), (15) and a β function (Eq. (1b) for EVV11; Eq. (2) for OEA13, Eq. (3) for D02 and Eq. (4b) for S05) form the core of each canopy exchange model configuration. Note that Eqs. (6)–(13) and (14b) are only required for the D02 model. Parameters for the photosynthesis model are representative of almond and the soil type is sand (parameterized using the C&H parameter set, see Table 2). Almond TRF was assumed to be most closely related to that of peach (both of the Prunus genus, see solid black line in Fig. 1, based on data of Do Paço et al., 2013) and this experiment was conducted on sandy soil under Mediterranean climatic conditions; hence this line, taken from Fig. 1, is shown again in Figs. 2 and 4 (this time as a grey solid line).

Fig. 2a illustrates that the TRF as calculated using the EVV11 model can take on a range of shapes, depending on which (combination of) pathways are used to apply water stress, and the degree of curvature in Eq. (1b). However, none of the curves manage to capture the shape of the peach TRF, that is typical of most isohydric plant species presented in Fig. 1 (apart maybe from Gynandropsis cv1).

Fig. 2b shows the TRFs obtained when the β-OEA13 is used, with the first 4 sets as proposed by the authors. These $\psi_{s,o}$ and $\psi_{s,c}$ values (see caption) bear no resemblance to soil matric potentials at FC or WP (both $\psi_{s,o}$ and $\psi_{s,c}$ are much 'drier' (more negative) than typical FC and WP values) which has led to the TRFs for PFT groups 1-4 being located much farther to the left than the data presented in Fig. 1.

However, the shape of the curves in Fig. 2b is much more promising than that presented in Fig. 2a, as result of the fact that Eq. (2) uses ψ_s, instead of θ, to calculate β. The best-fit PFT group uses $\psi_{s,o}$ and $\psi_{s,c}$ values that are far removed from the ones for
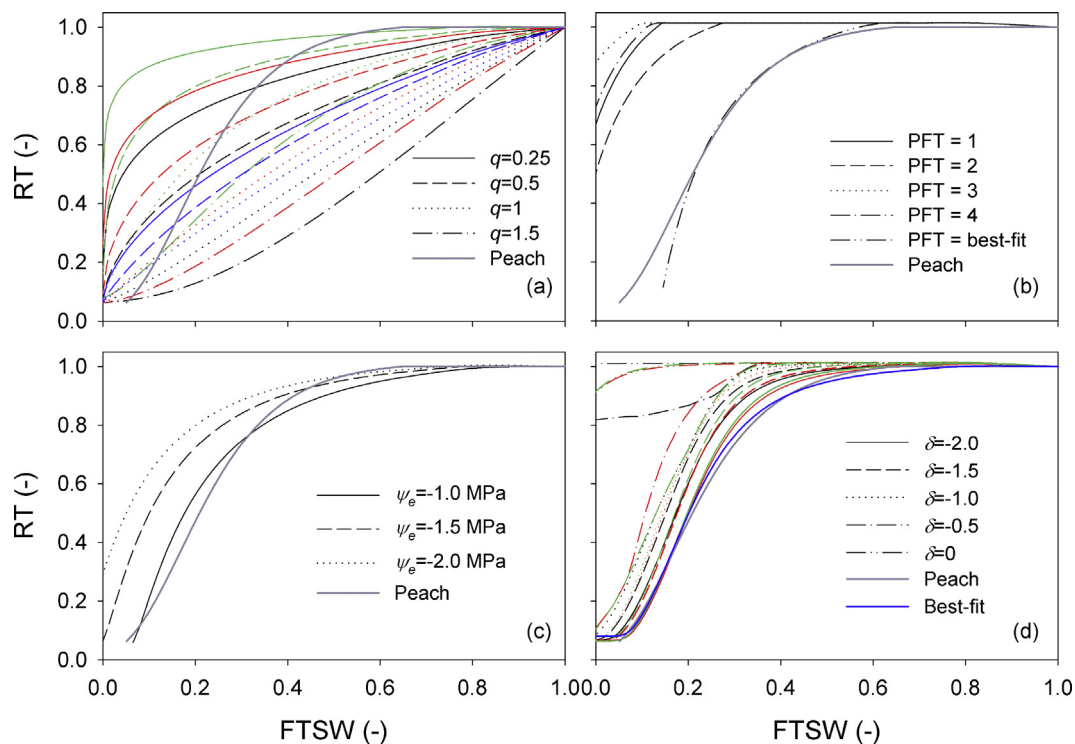
Fig. 2. TRFs for (a) EVV11 for stomatal (SL, black lines), biochemical (BL, red lines), or mesophyll (ML, green lines) limitation, with different degrees of curvature for β as denoted by q; the blue lines denote combinations of limitations, with solid blue line: $q_{SL} = 0.25$, $q_{BL} = 0.25$, $q_{ML} = 0.50$, dashed blue line: $q_{SL} = 0.5$, $q_{ML} = 0.5$, dotted blue line: $q_{SL} = 0.5$, $q_{BL} = 0.5$, (b) OEA13, PFT = 1: needleleaf trees and broadleaf evergreen trees ($\psi_{s,o} = -0.66$ and $\psi_{s,c} = -2.55$ MPa); PFT = 2: broad leaf deciduous trees ($\psi_{s,o} = -0.35$ and $\psi_{s,c} = -2.24$ MPa); PFT = 3: shrubs ($\psi_{s,o} = -0.83$ and $\psi_{s,c} = -4.28$ MPa); PFT = 4: C$_3$ and C$_4$ grasses and crops ($\psi_{s,o} = -0.74$ and $\psi_{s,c} = -2.75$ MPa); PFT = best-fit ($\psi_{s,o} = -0.1$ and $\psi_{s,c} = -0.7$ MPa), (c) S05 with ψ_e set to -1, -1.5 and 2.0 MPa and (d) D02, for $\delta = -2$, -1.5, -1, -0.5 and 0 MPa^{-1} and 3 options of where ABA-synthesis took place (leaf ABA: black lines; root ABA: red lines; both: green lines). The solid blue line ('best-fit') has L_{max} changed from 0.00667 to 0.0045 mol m^{-2} s^{-1} MPa^{-1}. Also shown in each plot are peach 'observations' taken from Fig. 1 (grey solid line).

the other 4 PFT groupings; however, these values are much closer to typical FC and WP values and when used in Eq. (2) we are able to approximately simulate the peach (sand) RT curve. Note that White et al. (2000), the publication CLM (OEA13) $\psi_{s,o}$ and $\psi_{s,c}$ values were based upon, list values of $\psi_{s,o} = -0.2$ and $\psi_{s,c}$ $-1.3/1.5$ MPa for *Acer saccharum* and *Juglans nigra*, also deciduous trees. These values (in particular $\psi_{s,o}$) are more in line with the best-fit parameter values we selected for Fig. 2b. Unfortunately, all of the $\psi_{s,o}$ and $\psi_{s,c}$ values, apart from those adopted for the two tree species mentioned above, are such in the White et al. (2000) paper (and hence in CLM) that they cause these uncharacteristically high relative transpiration values (see Fig. 2b) at the dry end of the FTSW range, which means that currently CLM will always overestimate transpiration when water stress occurs, for all PFTs.

In Fig. 2c, Eq. (4b) (simple S05 equation) has been employed to calculate β, with ψ_e set to the three values used by S05, representative of increasing plant water stress. The curve for $\psi_e = -1$ MPa approximates the measured peach RT values quite well. Like Eq. (2) this equation also uses ψ_s instead of θ, but requires only one parameter ('typical' ψ_e).

Finally, Fig. 2d shows the simulated RT values for the D02 model (with β given by Eq. (3)), with Eq. (9) selected to calculate R_{sr} (D02). Due to the relatively large number of plant parameters, this model is more flexible at representing the shapes of TRFs shown in Fig. 1. We tested the sensitivity to δ, which gives the degree of isohydricity (-2.0 to -0.5 MPa^{-1}), and whether ABA synthesis is taking place in leaves, roots or both (as affected by λ_e and λ_r). For these runs we used the standard values for the plant parameters proposed by D02 (see Table 1, but note that we adapted the value of ψ_e at which L_{re} falls to zero ($\psi_{xL} = -7$ MPa) based on evidence found in Cochard

et al., 2008), apart from the fact that we also varied δ (D02 fixed δ at -2.0 MPa^{-1}). The solid green line (both leaf and root synthesis, with $\delta = -2$ MPa^{-1}) approximates the peach TRF well, although it is slightly more placed to the left. However, by adjusting the L_{max} from 0.00667 to 0.0045 mol m^{-2} s^{-1} MPa^{-1}, we were able to get a very close fit between modeled and measured TRF (solid blue line; best-fit).

In addition, in Fig. 2d note the more S-shaped curve of the D02 model (convex at the onset of water stress, more concave thereafter). Model simulations by Metselaar and De Jong Van Lier (2007), who used a numerical analysis based on the differential equation describing radial flow to a single root, showed that a convex reduction function occurs shortly after the onset of limiting conditions, which may be explained by a transition period between the constant- and falling-rate phases. During the falling-rate phase the TRF is concave. They also found that the higher the root density, the more important this transition period, resulting in a convex reduction function (we will get back to this when discussing Fig. 4d). The EVV11 equation can take on a whole range of shapes between concave and convex (without varying root density, but by simply varying q), but cannot capture the combined convex-concave shape depicted in most curves presented in Fig. 1 (as represented by the peach curve in Fig. 2).

Fig. 2 illustrates the ability of the four proposed β models to approximate typical TRFs. The model that does poorly (EVV11), despite the fact that it is widely used in LSMs (with $q = 1$), has θ as its independent variable. The other models do relatively well with standard (S05) or slightly adapted parameter values (D02). OEA13 can only successfully approximate the RT versus FTSW curve when parameters are used that are well outside the range proposed by the authors.

The results shown in Fig. 2 were obtained for a sandy soil, with parameters for the calculation of FTSW (θ_{FC} and θ_{WP}) and K (for the D02 model), derived from the C&H soil hydraulic parameter set (see Table 2). In the remainder of this paper we will investigate what the effect is (on TRFs) of using different soil hydraulic parameterizations (B&C versus VGM) and hydraulic parameter sets. However, first the SWC and hydraulic conductivity curves will be discussed to illustrate the wide range of soil hydraulic properties resulting from the parameters summarized in Table 2.

3.2. Soil hydraulic properties

Fig. 3 shows ψ_s (a) and $\log_{10}(K)$ (b) as a function of effective soil moisture content, S_e (see Eq. (17)), a useful independent variable when SWCs for different textures are compared, for three soil textures (sand, loam and clay) and four soil hydraulic parameter sets (see Table 2). Overall, the sands (solid lines) are located on the far left of the plots, the loams (dashed lines) in the center, and the clays (dash-dotted lines) on the right. However, note the exception of the SVG clay SWC (blue dash–dotted line); it is ranked with the sands. There is also a large difference in K (e.g. $\sim$ a factor 1000 at field capacity, the highest K-value for each curve in Fig. 3b); K affects the soil-to-root resistance in Eq. (10). Fig. 3a and b are a good illustration of the large differences between the hydraulic parameter sets, i.e. their relative placement in the x–y domain and the slopes of the plots, e.g. a much flatter K–S_e curve for SVG loam and clay soils.

Apart from being affected by θ, values for β-EVV11, and hence TRF for EVV11, depend on FC and WP water contents, as well as on q-value (see Eq. (1b)). Values for θ_{FC} and θ_{WP} are given in Table 2, with generally the largest values for clays (save SVG) and lowest for sand. Note also the considerable differences between parameterizations within each texture group. β-S05, β-OEA13 and β-D02, on the other hand, depend on ψ_s; θ_{FC} and θ_{WP} do not play a role. For D02 the parameters that determine the K–θ curve are important as they determine the soil-to-root resistance, R_{sr} (see Eqs. (9) and (10)) and therefore related plant variables, such as root potential, ψ_r, leaf potential, ψ_e, and [ABA], which ultimately affect β-D02.

Figs. 3c and d plot ψ_s and $\log_{10}(K)$ as a function of FTSW (as this is the independent variable we use in the TRFs). Using FTSW, instead of S_e, as the independent variable concentrates the lines, in an order that is roughly similar to the one presented in Fig. 3a (note the sand SVG outlier). When $\log_{10}(K)$ is plotted as a function of FTSW (Fig. 3d), SVG loam and clay soils have the highest K-values at low FTSW values (<0.5); below FTSW = 0.4 the solid blue line (sand SVG) decreases sharply. Lowest K values (at all FTSW) are calculated for all WEA soil textures and for CEA sand.

Finally, although two of the four β parameterizations (OEA13 and S05) do not depend on the parameters presented in Table 2, the values of FTSW (= $(\theta - \theta_{WP})/(\theta_{FC} - \theta_{WP})$) do use θ_{FC} and θ_{WP}, and Table 2 shows that these values vary considerably per soil hydraulic parameter set. Hence, the curves presented in Fig. 2 will vary depending on soil texture, parameterization and parameter set (even if these parameters are not used directly in the β calculations). The soil effects on the TRFs will be discussed in the next section.

3.3. Modelled TRFs; sensitivity to soil parameter sets

Fig. 4a–d shows TRFs, for three different textures and four soil hydraulic parameter sets for the OEA13, S05 (Eq. (4b)), and D02 (R_{sr} from Eq. (9) (c) and R_{sr} from Eq. (10) (d)) plant water stress configurations, respectively. In this case the best-fit plant parameter sets (with regards to peach TRF data) have been selected for the soil sensitivity analysis. Note that no figure is shown for EVV11; for the EVV11 soil water stress configuration, all soil types, for all

soil hydraulic parameter sets, have the same β provided they have the same q value. This can be explained by the fact that FTSW = β for $q = 1$, and β depends non-linearly on FTSW when $q \neq 1$. This relationship is the same, independent of soil type or parameter set.

TRFs for OEA13 and S05 display little difference among soil hydraulic parameter sets apart from SVG sand (solid blue line). As expected, both models follow the same order as presented in Fig. 3c as ψ_s is the independent variable in Eqs. (2) and (4b).

In Figs. 3c and 4a and b, the sand curves (solid lines) are located furthest to the left (in particular sand SVG), indicating that according to these β models plants in sandy soils would experience less water stress than finer-textured soils at any FTSW value, as also found by S05, who employed C&H in his model analyses involving Eqs. (4a) and (4b). However, for Lotus in Fig. 1 we find the order (from left to right) loam, clay, then sand, the opposite to Fig. 4a and b.

Note that S05 used Eqs. (4a) and (4b) to directly calculate RT whereas we used 4b to find β, then RT; however, the order of curves would not change and the values of β versus FTSW are only slightly different from RT values (because surface temperature for well-watered and droughted plants differed by up to about 1.5 °C only).

Fig. 4c shows the soil texture sensitivity analysis for the D02 model (with Eq. (9), D02's original, used to calculate R_{sr}). Here, all WEA (green) and the loam and sand SVG curves are very different from the other curves that approximate the experimental peach TRF. The WEA sand curve is not shown, and the WEA curves for the other two soil types are only part-shown, because its β values (calculated from Eq. (3)) reached zero very soon. As pointed out in Section 2.1, Eq. (9) for R_{sr} is equivalent to $R_{sr,min}(K_{sat}/K(\theta))$, so that (when inserting Eq. (18) or 20 for $K(\theta)$) the absolute values of K_{sat} are not used, but only those that determine the shape of the $K(\theta)$ curve (b and $\psi_{s,sat}$ for B&C and l and m for VGM). For the WEA and SVG sand and loam parameter sets these parameters are such that they cause R_{sr} values to become very high, already at small negative ψ_s values, thereby causing β-D02 to reach near-zero values at all (for sand) or relatively high FTSW values.

However, Fig. 4c does have a more plausible order of those curves that approximately follow the shape of the peach TRF: for the B&C parameterization (C&H and CEA parameter set) the order is clay, loam, sand, which fits much better with the Lotus experimental ranking in Fig. 1, and is also supported by the modeling study of Metselaar and De Jong Van Lier (2007).

Fig. 4d shows TRFs when Eq. (10) is used to calculated R_{sr} (note that in this case $R_{sr,min}$ does not play a role). Here γ_{ABA} was set to 8×10^{-4} m^3 mol^{-1} ABA, and L_{max} to 0.004 mol m^{-2} s^{-1} MPa^{-1}, to ensure the best fit with the experimental peach TRF for C&H sand (but note that the fit is not as good as when Eq. (9) was used for R_{sr}). There is a large spread in TRF among the different soil hydraulic parameterizations, that clearly rank with K (see Fig. 3d), because K is an explicit variable in Eq. (10), but also with the positioning of the ψ_s versus FTSW curves (as ψ_s is strongly related to ψ_r and ψ_e in D02), for example the sand SVG TRF being placed so far to the left. R_{sr} calculated from Eq. (10) is affected by root-geometry dependent values r, d (Eq. (11)) and L_a (Eq. (12)). Hamblin and Tennant (1987), for example, list L_a data ranging between 100 (broad bean) and 2300 (wheat) m^{-1}, so our 299 is a plausible value. Sensitivity tests (not shown) with different combinations of r, d and L_a showed that the order, shape and spread of the curves in Fig. 4d were relatively little affected, indicating that the effect of changes in the magnitude of K were much more pertinent. However, in line with the results shown by Metselaar and De Jong Van Lier (2007), larger values of L_a increased the convexity of the curve and moved the TRF to the left, in particular for the clay soil (for tests with C&H soils, data not shown).
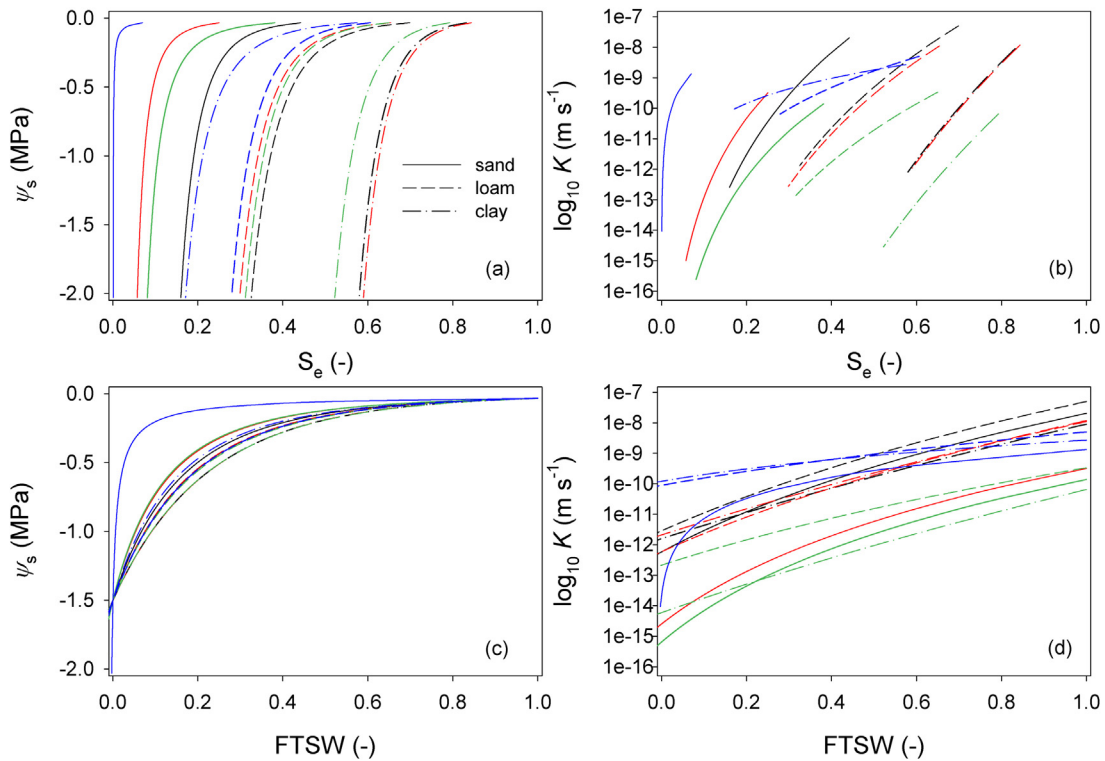
Fig. 3. (a) SWC: soil matric potential, ψ_s, versus effective saturation, S_e, and (b) hydraulic conductivity, K (logarithmic scale) versus S_e for three soil textural types (solid, sand; dashed, loam; dash–dotted, clay) and four hydraulic parameter sets (black: C&H; red: CEA; green: WEA; blue: SVG), (c) ψ_s and (d) $\log_{10} K$ as a function of FTSW.

S05 analysed the predicted response of *RT* to FTSW (using Eq. (4a)) and showed that it was relatively insensitive to soil hydraulic conductivity, θ_{FC} and θ_{WP}, and ψ_e. However, the large spread in Fig. 4c and d illustrates that with the D02 β parameterization, some soil parameter sets (in particular those for sands and for the VGM equations) can yield improbable *RT* values, as the calculated impact of soil texture on the TRF is large. With this in mind, C&H would be the best soil parameter set to represent transpiration responses
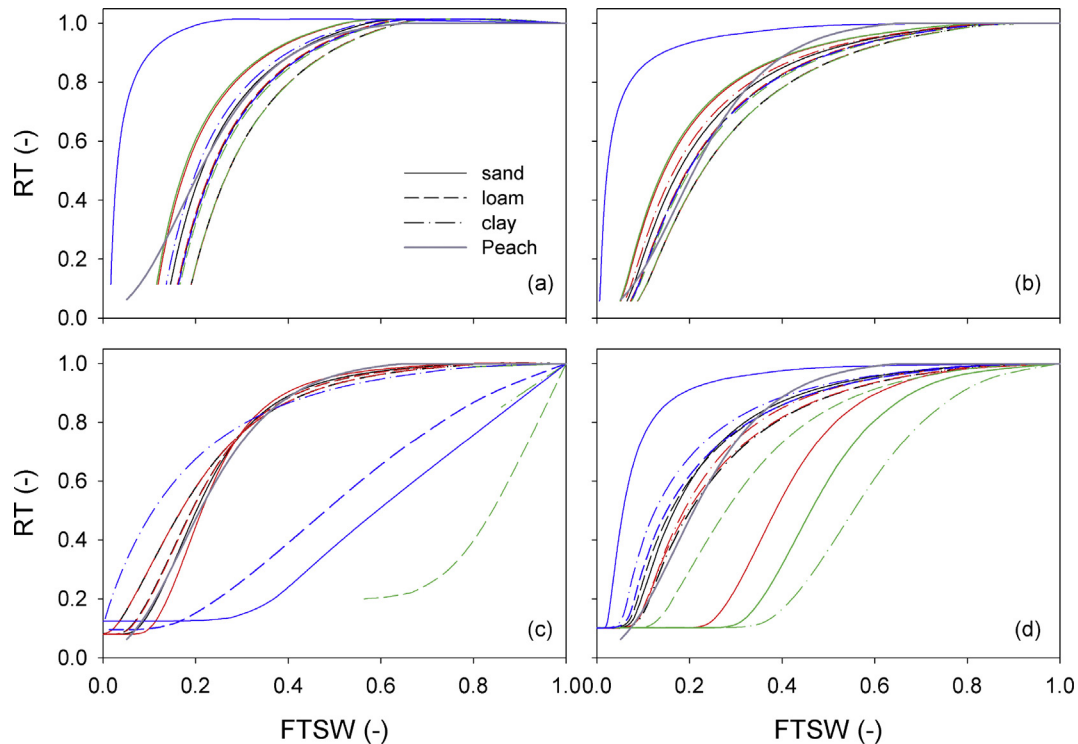

Fig. 4. TRFs for three soil types and four different soil hydraulic parameter sets (see Fig. 3) for (a) OEA13 with PFT = best-fit, (b) S05, with $\psi_e = -1.0$ MPa, (c) D02 using Eq. (9) to calculate R_{sr} and best-fit parameters (see caption of Fig. 2), (d) D02 using Eq. (10) to calculate R_{sr} and best-fit parameters ($\gamma_{ABA} = 8 \times 10^{-4}$ m^3 mol^{-1} ABA and $L_{max} = 0.004$ mol m^{-2} s^{-1} MPa^{-1}).

to drying soil, as the influence of soil texture on the abovementioned relationship is much more reduced than with the rest of parameterizations.

The observed variations in the FTSW threshold in drying soil for declining transpiration rate (Fig. 1) is an important plant trait linked to drought resistance capacity, lately used in breeding programs to improve crops' drought resistance (Gholipoor et al., 2013). A major limitation of the S05 approach, and to a certain degree of OEA13, is that these species-specific variations of the TRF cannot be predicted, as ψ_e (kept constant) is its only plant-specific parameter and it has been shown to play a limited role on the shape of this relationship (Sinclair, 2005). A key advantage of the D02 β model is that species-specific differences in the transpiration response to drying soil can be modeled by changing the value of three physiological parameters: L_{max}, γ and δ (as well as root density, see above). Sensitivity analyses for these three parameters (data not shown) indicate that the threshold FTSW in drying soil that triggers the start of the drop in RT is displaced when the parameter values change. When γ (parameter expressing g_s sensitivity to [ABA]) increases, the FTSW value that triggers rapid RT reductions also increases. The same happens with decreasing L_{max} values indicating that species with lower maximum xylem hydraulic conductivities and/or higher sensitivities of g_s to [ABA] are more water conservative and more prone to withstand persisting drought events. In the case of δ, a parameter involved in invoking an isohydric ($\delta < 0$) or anisohydric ($\delta = 0$) response, the FTSW threshold value decreases as its value increases and approaches zero for $\delta = 0$. These responses agree with experimental evidence that isohydric species are more water-conservative and may present some advantages in dry ecosystems (Sade et al., 2012).

4. Conclusions

Plant water stress models that have ψ_s as their independent variable produce a more realistic transpiration reduction function, TRF (relative transpiration, RT, versus fraction of transpirable soil water, FTSW) than those based on θ. Out of the three models we tested that use ψ_s, two relatively empirical (with one and two leaf water potential-related parameters, respectively) and one involving chemical and hydraulic signaling (D02), the latter one was most successful at reproducing TRFs found in experimental studies. Metselaar and De Jong Van Lier (2007), who used a numerical analysis based on the differential equation describing radial flow to a single root, also found the combined convex-concave reduction function shape, obtained experimentally, that is successfully replicated by the D02 model.

Furthermore, the D02 parameterization is more flexible due to the fact it has three key plant parameters that can be varied, based on plant physiological considerations linked to degree of isohydricity, maximum xylem hydraulic conductivity and sensitivity of g_s to [ABA]. When parameters related to root configuration are considered in the soil-to-root resistance, its flexibility is further increased.

However, because of the way soil hydraulic conductivity, K, affects its root-to-soil hydraulic resistance, and related knock-on effect on calculated values of root and leaf water potential, the more mechanistic method is very sensitive to soil hydraulic parameters used to describe the magnitude of K and the shape of the K versus θ function, leading to unrealistic $g_s/g_{s,max}$ and E/E_{max} values, for in particular the Van Genuchten-Mualem type of equations.

Nevertheless, for the more robust Brooks and Corey-type soil parameter sets (Clapp and Hornberger, 1978 and Cosby et al., 1984) the model predicted a ranking of transpiration reduction functions, as affected by soil texture, that was more in tune with what has been observed experimentally than that predicted by the empirical ψ_s-based models.

In the θ-based water stress model, soil texture (or hydraulic parameterization, for that matter) did not affect the transpiration reduction function, which is unrealistic.

In light of these findings we only recommend complex hydraulic and chemical signaling models to be implemented in land surface models, if combined with the B&C-type soil hydraulic parameterization and reliable soil hydraulic (and plant) parameters. Furthermore, operational implementation of these equations will first require in-depth testing and bench-marking studies for a range of vegetation types involving off-line and coupled land surface-atmosphere simulations. Only then can it be determined whether these physiologically more detailed models are indeed more successful at predicting the intricate interactions between the water-, energy- and carbon balance under current and future climatic conditions.

Acknowledgements

References

Arora, V.K., 2003. Simulating energy and carbon fluxes over winter wheat using coupled land surface and terrestrial ecosystem models. Agric. For. Meteorol. 118, 21–47.

Best, M., Pryor, M., Clark, D., Rooney, G., Essery, R., Ménard, C., Edwards, J., Hendry, M., Porson, A., Gedney, N., Mercado, L., Sitch, S., Blyth, E., Boucher, O., Cox, P., Grim- mond, C., Harding, R., 2011. The Joint UK Land Environment Simulator (JULES), Model description—part 1: energy and water fluxes. Geosci. Model Dev. Discuss. 4, 595–640.

Boussetta, S., Balsamo, G., Beljaars, A., Agusti-Panareda, A., Calvet, J.-C., Jacobs, C., van den Hurk, B., Viterbo, P., Lafont, S., Dutra, E., Jarlan, L., Balzarolo, M., Papale, D., van der Werf, G., 2013. Natural land carbon dioxide exchanges in the ECMWF Integrated Forecasting System: Implementation and offline validation. J. Geophys. Res. Atmos. 118, http://dx.doi.org/10.1002/jgrd.50488.

Brooks, R.H., Corey, A.T., 1964. Hydraulic Properties of Porous Media, 3. Colorado State University Hydrology Papers, Fort Collins, USA.

Calvet, J.-C., 2000. Investigating soil and atmospheric plant water stress using physiological and micrometeorological data. Agric. For. Meteorol. 103, 229–247.

Calvet, J.C., Rivalland, V., Picon-Cochard, C., Guehl, J.M., 2004. Modelling forest transpiration and CO$_2$ fluxes—response to soil moisture stress. Agric. For. Meteorol. 124, 143–156.

Clapp, R.B., Hornberger, G.M., 1978. Empirical equations for some soil hydraulic properties. Water Resour. Res. 14, 601–604.

Cochard, H., Barigaha, S.T., Kleinhentz, M., Eshel, A., 2008. Is xylem cavitation resistance a relevant criterion for screening drought resistance among Prunus species? J. Plant Physiol. 165, 976–982.

Cosby, B.J., Hornberger, G.M., Clapp, R.B., Ginn, T.R., 1984. A statistical exploration of the relationships of soil moisture characteristics to the physical characteristics of soils. Water Resour. Res. 20, 682–690.

De Jong van Lier, Q., van Dam, J., Durigon, A., dos Santos, M.A., 2013. Metselaar, modeling water potentials and flows in the soil–plant system comparing hydraulic resistances and transpiration reduction functions. Vadose Zone J. 12, http://dx.doi.org/10.2136/vzj2013.02.0039.

Dewar, R.C., 2002. The Ball–Berry–Leuning and Tardieu–Davies stomatal models: synthesis and extension within a spatially aggregated picture of guard cell function. Plant Cell Environ. 25, 1383–1398.

Diaz-Espejo, A., Verhoef, A., Knight, R., 2005. Illustration of micro-scale advection using grid-pattern mini-lysimeters. Agric. For. Meteorol. 129, 39–52.

Do Paço, T.A., Ferreira, M.I., Pacheco, C.A., 2013. Scheduling peach orchard irrigation in water stress conditions: use of relative transpiration and predawn leaf water potential. Fruits 68, 147–158.

Durigon, A., Santos, M.A., dos Lier, Q.D., van Metselaar, K., 2012. Pressure heads and simulated water uptake patterns for a severely stressed bean crop. Vadose Zone J. 11 (2012)3. -ISSN 1539-1663.

Egea, G., Verhoef, A., Vidale, P.L., 2011a. Towards an improved and more flexible representation of water stress in coupled photosynthesis–stomatal conductance models. Agric. For. Meteorol. 151, 1370–1384.

Egea, G., Verhoef, A., González-Real, M.M., Baille, A., Nortes, P.A., Domingo, R., 2011b. Comparison of several approaches to modelling stomatal conductance in well-watered and drought-stressed almond trees. Acta Hort. (ISHS) 922, 285–293.

Farquhar, G.D., von Caemmerer, S., Berry, J.A., 1980. A biochemical model of photosynthetic CO_2 assimilation in leaves of C_3 species. Planta 149, 78–90.

Feddes, R.A., Kowalik, P.J., Zaradny, H., 1978. Simulation of field water use and crop yield. In: Simulation Monograph Series. PUDOC, Wageningen, The Netherlands.

Fernandez-Galvez, J., Verhoef, A., Barahona, E., 2007. Estimating soil water fluxes from soil water records obtained using dielectric sensors. Hydrol. Process. 21, 2785–2793.

Gardner, W.R., Ehlig, C.F., 1963. The influence of soil water on transpiration by plants. J. Geophys. Res. 68, 5719–5724.

Gholipoor, M., Sinclair, T.R., Vara Prasad, P.V., 2012. Genotypic variation within sorghum for transpiration response to drying soil. Plant Soil 357, 35–40.

Gholipoor, M., Sinclair, T.R., Raza, M.A.S., Löffler, C., Cooper, M., Messina, C.D., 2013. Maize hybrid variability for transpiration decrease with progressive soil drying. J. Agron. Crop Sci. 199, 23–29.

Gregory, P., Nortcliff, S. (Eds.), 2013. Soil Conditions and Plant Growth. , 12th ed. Wiley-Blackwell, Chichester, UK, p. 461.

Hamblin, A.P., Tennant, D., 1987. Root length density and water uptake in cereals and grain legumes: how well are they correlated? Austr. J. Agric. Res. 38, 513–527.

Jacobs, C.M.J., 1994. Direct impact of atmospheric CO_2 enrichment on regional transpiration. Agricultural University of Wageningen. Ph.D. thesis.

Keenan, T., Garcia, R., Friend, A.D., Zaehle, S., Gracia, C., Sabate, S., 2009. Improved understanding of drought controls on seasonal variation in Mediterranean forest canopy CO_2 and water fluxes through combined in situ measurements and ecosystem modeling. Biogeosciences 6, 1423–1444.

Kozlowski, T.T., Kramer, P.J., Pallardy, S.G., 1991. The Physiological Ecology of Woody Plants. Academic Press, San Diego, pp. 657.

Krinner, G., Viovy, N., Noblet-Ducoudre, N., Ogée, J., Polcher, J., Friedlingstein, P., Ciais, P., Sitch, S., Prentice, I.C., 2005. A dynamic global vegetation model for studies of the coupled atmosphere-biosphere system. Global Biogeochem. Cycles 19, GB1015.

Leuning, R., 1995. A critical appraisal of a combined stomatal-photosynthesis model for C_3 plants. Plant Cell Environ. 18, 339–355.

Marshall, T.J., Holmes, J.W., Rose, C.W., 1996. Soil Physics, 3rd ed. CUP, Cambridge, UK.

Marthews, T.R., Quesada, C.A., Galbraith, D.R., Malhi, Y., Mullins, C.E., Hodnett, M.G., Dharssi, I., 2014. High-resolution hydraulic parameter maps for surface soils in tropical South America. Under review in Geoscientific Model Development (http://www.geosci-model-dev-discuss.net/6/6741/2013/gmdd-6-6741-2013.html).

Masinde, P.W., Stützel, H., Agong, S.G., Fricke, A., 2005. Plant growth, water relations, and transpiration of Spiderplant [*Gynandropsis gynandra* L. Briq.] under water limited conditions. J. Am. Soc. Hort. Sci. 130, 469–477.

Metselaar, K., De Jong Van Lier, Q., 2007. The shape of the transpiration reduction function under plant water stress. Vadose Zone J. 6, 124–139.

Metselaar, K., Sinclair, T.R., 2005. Letters to the Editor: Comment on "Theoretical Analysis of Soil and Plant Traits Influencing Daily Plant Water Flux on Drying Soils" by T.R. Sinclair. Agron. J. 97, 1148–1152;
Metselaar, K., Sinclair, T.R., 2005. Letters to the Editor: Comment on "Theoretical Analysis of Soil and Plant Traits Influencing Daily Plant Water Flux on Drying Soils" by T.R. Sinclair. Agron. J. 99, 1188–1189.

Mualem, Y., 1976. A new model predicting the hydraulic conductivity of unsaturated porous media. Water Resour. Res. 12, 513–522.

Mullins, C.E., 2001. Matric potential. In: Smith, K.A., Mullins, C.E. (Eds.), Soil and Environmental Analysis: Physical Methods. , 2nd ed. Marcel Dekker, New York, pp. 65–93.

Oleson, K., D.M. Lawrence, G.B. Bonan, B. Drewniak, M. Huang, C.D. Koven, S. Levis, F. Li, W.J. Riley, Z.M. Subin, S. Swenson, P.E. Thornton, A. Bozbiyik, R. Fisher, C.L. Heald, E. Kluzek, J.-F. Lamarque, P.J. Lawrence, L.R. Leung, W. Lipscomb, S.P. Muszala, D.M. Ricciuto, W.J. Sacks, Y. Sun, J. Tang, Z.-L. Yang, 2013. Technical description of version 4.5 of the Community Land Model (CLM). NCAR Technical Note NCAR/TN-503+STR, 420 pp., DOI: 10.5065/D6RR1W7M.

Ronda, R.J., de Bruin, H.A.R., Holtslag, A.A.M., 2001. Representation of the canopy conductance in modeling the surface energy budget for low vegetation. J. Appl. Meteorol. 40, 1431–1444.

Sade, N., Gebremedhin, A., Moshelion, M., 2012. Risk-taking plants: anisohydric behavior as a stress resistance trait. Plant Signal. Behav. 7, 767–770.

Sadras, V.O., Milroy, S.P., 1996. Soil–water thresholds for the responses of leaf expansion and gas exchange: a review. Field Crops Res. 47, 253–266.

Sala, A., Tenhunen, J.D., 1996. Simulations of canopy net photosynthesis and transpiration in Quercus ilex L under the influence of seasonal drought. Agric. For. Meteorol. 78, 203–222.

Saxton, K.E., Rawls, W.J., Romberger, J.S., Papendick, R.I., 1986. Estimating generalized soil–water characteristics from texture. Soil Sci. Soc. Am. J. 50, 1031–1037.

Schaap, M.G., Van Genuchten, M.T., 2006. A modified Mualem-van Genuchten formulation for improved description of the hydraulic conductivity near saturation. Vadose Zone J. 5, 27–34.

Sellers, P.J., Randall, D.A., Collatz, G.J., Berry, J.A., Field, C.B., Dazlich, D.A., Zhang, C., Collelo, G.D., Bounoua, L., 1996. A revised land surface parameterization (SiB2) for atmospheric GCMs, 1. Model formulation. J. Clim. 9, 676–705.

Sinclair, T.R., 2005. Theoretical analysis of soil and plant traits influencing daily plant water flux on drying soils. Agron. J. 97, 1148–1152.

Sinclair, T.R., Holbrook, N.M., Zwieniecki, M.A., 2005. Daily transpiration rates of woody species on drying soil. Tree Physiol. 25, 1469–1472.

Tardieu, F., Bruckler, L., Lafolie, F., 1992. Root clumping may affect the root water potential and the resistance to soil–root water transport. Plant Soil 140, 291–301.

Tardieu, F., Davies, W.J., 1993. Integration of hydraulic and chemical signalling in the control of stomatal conductance and water status of droughted plants. Plant Cell Environ. 16, 341–349.

Tardieu, F., Lafarge, T., Simonneau, T., 1996. Stomatal control by fed or endogenous xylem ABA in sunflower: Interpretation of correlations between leaf water potential and stomatal conductance in anisohydric species. Plant Cell Environ. 19, 75–84.

Tardieu, F., Simonneau, T., 1998. Variability among species of stomatal control under fluctuating soil water status and evaporative demand: modelling isohydric and anisohydric behaviours. J. Exp. Bot. 49, 419–432.

Thornley, J.H.M., Johnson, I.R., 1990. Plant and Crop Modelling. Clarendon Press, Oxford, UK.

Van Dam, J.C., Groenendijk, P., Hendriks, R.F.A., Kroes, J.G., 2008 May. Advances of modeling water flow in variably saturated soils with SWAP. Vadose Zone J. 7 (2).

Van Den Hoof, C., Vidale, P.L., Verhoef, A., Vincke, C., 2013. Improved evaporative flux partitioning and carbon flux in the land surface model JULES: Impact on the simulation of land surface processes in temperate Europe. Agric. For. Meteorol. 181, 108–124.

Van Genuchten, M.Th., 1980. A closed-form equation for predicting the hydraulic conductivity of unsaturated soils. Soil Sci. Soc. Am. J. 44, 892–898.

Veihmeyer, F.J., Hendrickson, A.H., 1931. The moisture equivalent as a measure of the field capacity of soils. Soil Sci. 32 (3), 181–193.

Verhoef, A., Egea, G., 2013. Chapter 9—soil water and its management. In: Gregory, P., Nortcliff, S. (Eds.), 2013. Soil Conditions and Plant Growth. , 12th ed. Wiley-Blackwell, Chichester, UK, p. 461.

White, M.A., Thornton, P.E., Running, S.W., Nemani, R.R., 2000. Parameterization and sensitivity analysis of the Biome-BGC terrestrial ecosystem model: net primary production controls. Earth Interact. 4, 1–85.

Wösten, J.H.M., Lilly, A., Nemes, A., Le Bas, C., 1999. Development and use of a database of hydraulic properties of European soils. Geoderma 90, 169–185.

Zampieri, M., D'Andrea, F., Vautard, R., Ciais, P., De Noblet-Ducoudre, N., Yiou, P., 2009. Hot European summers and the role of soil moisture in the propagation of Mediterranean drought. J. Clim. 22, 4747–4758.